FEATURE ARTICLE

Hot spots in different metal nanostructures for plasmon-enhanced Raman spectroscopy

Hong Wei and Hongxing Xu*

Noble metal nanostructures are able to concentrate light into small volumes, which enhances greatly the local electromagnetic (EM) field near the metal nanostructures. The areas with greatly enhanced EM field become "hot spots" for surface-enhanced Raman spectroscopy (SERS), which utilizes the field enhancement properties of metal nanostructures to amplify the usually weak Raman scattering signals. The preparation of metal nanostructures with superior SERS performances is one of the main topics in the SERS field and is important for the applications of SERS in sensing and analysis. In this feature article, we review several different kinds of metal structures for SERS, including coupled metal nanostructures, nanostructure arrays, nano/micro structures with textured surfaces and graphene-mediated SERS substrates. Tip-enhanced Raman spectroscopy (TERS) using the metal tip of the scanning tunneling microscope is also discussed. Besides the intensity enhancement in SERS and TERS, some less studied aspects are highlighted; for example, the remote excitation technique, tuning the nanogap of gold nanorod dimers through strain control on an elastomeric substrate, manipulating Raman emission polarization using asymmetric nanoantennas, and investigating plasmon-enhanced chemical reactions by TERS.

1 Introduction

Since its discovery in the 1970s, surface-enhanced Raman scattering/spectroscopy (SERS) has attracted researchers' interest to understand the enhancement mechanism and fabricate different kinds of substrates for SERS applications.[1–3] Electromagnetic (EM) field enhancement resulting from the excitation of surface plasmons on metal surfaces in most cases contributes dominantly to the Raman enhancement. The EM field enhancement effect is particularly pronounced in nanogaps between coupled structures. Dimers of metal nanoparticles (NPs) are simple and effective structures to generate a greatly enhanced Raman signal, which were first used to reveal definitely the EM field enhancement mechanism in single molecule SERS.[4–7] The area with a strongly enhanced EM field is called a "hot spot". Usually the size of the hot spot is tiny compared with the volume of the nanostructure, but most of the experimentally obtained SERS signals are generated in the tiny hot spots. Recent researches regarding the NP dimer or larger nanoaggregates have been devoted to fabricating those structures in controllable ways. Assemblies using chemical linkers or coatings have been reported by different groups.[8,9] Plasmon-enhanced optical forces have been demonstrated to create NP dimers for SERS.[10,11]

Besides nanospheres, nanoparticles of different geometries have been used to enhance Raman scattering. For nanocubes, the hot spots can be formed between two nanocubes in the configurations of face-to-face, edge-to-edge, and edge-to-face. The different coupling geometries of nanocube dimers lead to different Raman enhancements.[12,13] The sharp corners of the nanocubes can also generate an enhanced EM field for SERS. In general, sharp protrusions in metal nanostructures can provide hot spots,[5] for instance, nanostars, nanorice and bipyramids.[14–17] By mimicking hot spot generation in nanosphere aggregates, various structures have been explored by transforming nanospheres to triangles,[18] nanodisks,[19] and nanorods.[20] In core–shell nanostructures, the space between the core and shell provides large-volume hot spots.[21] Complex NP aggregates were also made to provide hot spots.[22,23] By using nanofabrication techniques or self-assembly methods, ordered NP arrays have also been prepared for SERS measurements.[24–27] By depositing metal NPs onto nanowire arrays, a three dimensional SERS substrate was obtained.[28]

As Raman spectra can reveal the structural information of analytes, Raman spectroscopy is an important technique for detection and analysis. Due to its high sensitivity, SERS has greatly widened the area of application of Raman spectroscopy. SERS has been intensively explored for chemo- and bio-sensing. For instance, SERS was used to capture the conformational changes of single photoactive yellow protein molecules under photoexcitation,[29] and probe the Raman signal of molecules in living cells.[30,31] SERS also provides effective real time

Beijing National Laboratory for Condensed Matter Physics and Institute of Physics, Chinese Academy of Sciences, Box 603-146, Beijing 100190, China. E-mail: hxxu@iphy.ac.cn

monitoring of chemical reactions.[32] To generalize the application of SERS, the preparation of metal nanostructures with superior performances for SERS is critical and highly desired.

In this feature article, we review some recent developments in the preparation of superior SERS substrates. In Section 2, different coupled nanostructures are presented. Besides the Raman enhancement achieved in these structures, some rarely studied aspects of SERS are discussed. For example, the remote excitation method based on the wire–particle system is introduced, which shows several advantages compared with traditional experimental methods and may find applications in special circumstances; nanorod dimers on elastomeric substrates realize the systematic examination for a single structure with different gap sizes; asymmetric NP aggregates function as antennas to manipulate the polarization of the Raman signal. In Section 3, we aim at the SERS performances of metal nanostructure arrays, usually prepared by using top-down fabrication techniques or template-assisted fabrication processes. In Section 4, the developments of metal structures with rough surfaces and their performances for SERS are briefly reviewed. In Section 5, a newly developed SERS substrate, which incorporates a metal nanostructure and graphene, is discussed. In Section 6, we discuss an enhancement scheme utilizing the metal tip of scanning probe microscopy and its recent application in studying plasmon-enhanced chemical reactions. Finally, we summarize this article and give tentative outlook.

2 Coupled nanostructures for Raman enhancement

2.1 Dimers of asymmetric geometries

The electromagnetic coupling between metal NPs can generate a greatly enhanced EM field in the junction of the coupled structures, which makes those structures efficient for the enhancement of the Raman signal of the probe molecules. Metal NP dimers are intensively investigated for their enhancement mechanism and SERS performances. Nanohole arrays in metal films have also been used for SERS.[33–35] Due to the weak field-enhancement of isolated single holes, they cannot enhance efficiently the Raman scattering. The holes provide the cavity to hold other structures. By using chemical modification of the sample surface, gold NPs can be put into the nanoholes in a gold film. The composite nanohole–nanoparticle forms a novel coupled structure for SERS applications.[36] Fig. 1a shows scanning electron microscopy (SEM) images of the hole–particle pairs. Depending on the experimental conditions and the relative sizes of the hole and particle, more than one particle can be placed into a single hole. The space between the nanoparticle and the wall of the nanohole forms "hot spots" with a strongly enhanced electric field. Therefore, this structure can greatly enhance the Raman signal intensity. Fig. 1b shows the spectra of malachite green isothiocyanate (MGITC) molecules from a hole–particle pair and from a single hole. The spectrum from the coupled structure shows much higher Raman intensity. The electric field distributions calculated using a finite-difference time-domain (FDTD) method confirm the large electric field enhancement in the junction between the
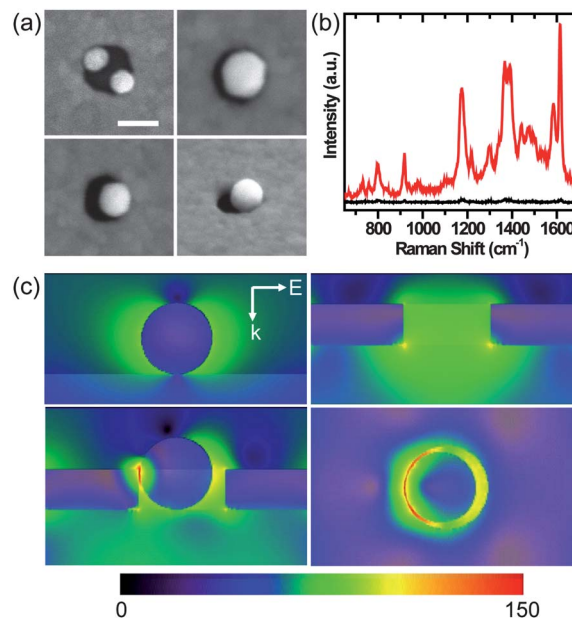

Fig. 1 (a) SEM images of Au nanohole–nanoparticle structures. The length of the scale bar is 100 nm. (b) The SERS spectra of MGITC molecules measured from the hole–particle pair (red curve) and from single hole (black curve). (c) The calculated electric field amplitudes for a single nanoparticle, single nanohole and coupled hole–particle structure. The diameter of the nanoparticle and nanohole is 100 nm and 120 nm, respectively. The smallest separation between the nanoparticle and the nanohole is 3 nm. The excitation wavelength is 633 nm. (Reproduced from ref. 36.)

hole and the particle (Fig. 1c). For a Au NP of 100 nm diameter located in a hole of 120 nm diameter in an Au film of 55 nm thickness, the maximum electric field enhancement is 147 for a separation of 3 nm, which corresponds to Raman enhancement of about 4.7×10^8. One prominent advantage of the hole–particle structure is that the "hot spot" in this structure has a much larger volume, as can be seen from the right bottom panel in Fig. 1c, which cannot be obtained in NP dimers due to curvature differences. Huang *et al.* investigated by simulation the field enhancement factor and resonant wavelength as a function of the separation between a gold NP and the void in a gold film, and experimentally showed that a strong SERS signal can be obtained from this kind of coupled structure.[37]

Another type of asymmetric coupled structure for SERS is the nanowire (NW)–nanoparticle (NP) structure (Fig. 2a). The junction between the NW and the NP provides the hot spot with greatly enhanced electric field when the excitation laser light is polarized perpendicular to the NW (Fig. 2b, left). When the laser is polarized parallel to the NW, the electric field intensity at the junction is much weaker (Fig. 2b, right). The polarization dependence of the electric field results in the polarization dependence of the SERS signal. Fig. 2c shows the variation of the SERS intensity with the change of the laser polarization. As can be seen, the Raman signal was the strongest for the laser light polarized perpendicular to the NW and the weakest for parallel polarization. In this structure, it was found that the SERS intensity is proportional to $\cos^2 \theta$ instead of $\cos^4 \theta$ (the definition of θ is shown in Fig. 2b), because the enhancement
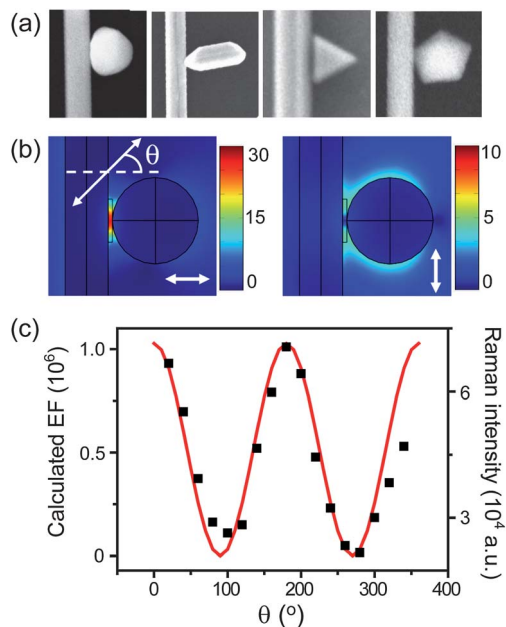
Fig. 2 (a) SEM images of coupled Au nanowire–nanoparticle structures. (b) The calculated electric field amplitudes for a gold sphere of radius 50 nm at 5 nm from a wire of radius 25 nm for excitation light polarization perpendicular (left) and parallel (right) to the nanowire. The excitation wavelength is 633 nm. (c) The calculated enhancement factor (EF) of SERS (red curve) and experimentally measured SERS intensity (black squares) as a function of the polarization angle of the excitation light. (Reproduced from ref. 38.)
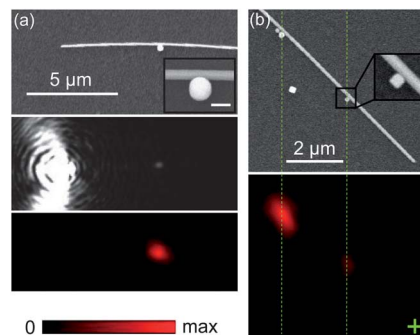

Fig. 3 (a) Remote SERS in a structure with one hot spot. Top: SEM images; middle: laser light scattering image; bottom: Raman image. (b) Remote SERS in a structure with multiple hot spots. Top: SEM images; bottom: Raman image. (Reproduced from ref. 41.)

factor of excitation field is proportional to $\cos^2 \theta$ while the Raman emission enhancement is polarization-independent.[38] The coupled NW–NP structure has been employed for DNA sensing.[39]

Metal nanowires can function as waveguides to transmit light at lateral dimensions of the subwavelength scale, which has attracted much attention and the properties of plasmonic nanowires have been intensively studied.[40] In the coupled NW–NP structure, the NP can function as an antenna to convert the propagating surface plasmons to photons which can be detected by light scattering at the far field. By illuminating the end of the NW, a hot spot at the NW–NP junction can also be generated. Therefore, remote excitation of SERS can be conceived.[41,42] In experiments, a silver NW–NP structure was used (Fig. 3a). Laser light of 633 nm wavelength was focused onto the left end of the NW. The bright spot at the NP location (middle panel in Fig. 3a) indicates propagating plasmons were launched on the NW. By imaging with the Raman signal of the probe molecule, strong Raman signal was detected at the NW–NP junction (bottom panel in Fig. 3a). The extremely low molecule concentration used in our sample preparation suggests that the remotely excited SERS signal probably originates from single molecules in the NW–NP junction, which means this remote-excitation technique has sensitivity at the single molecule level. Compared with the ordinary excitation configuration, the remote excitation is advantageous. The hot spot at the NW–NP junction is remotely excited, so the excitation area is of nanoscale dimensions, which avoids background

noise due to a large excitation area and lowers the possible damages to the sample caused by the strong laser intensity. The remote-excitation method provides a new way to perform sensing measurements based on surface-enhanced optical signals and may find applications in systems where the normal excitation method is unsuitable. If more than one junction is present on the nanowire, multiple hot spots can be excited simultaneously by the remote excitation method (Fig. 3b).

Metal nanoparticles over a metal mirror (NPOM) form an asymmetric coupled structure which is an effective SERS substrate (Fig. 4a).[43] Au film was first deposited on a SiO$_2$/Si substrate. Then a dielectric layer, e.g. SiO$_2$, was deposited covering the Au film by using the atomic layer deposition (ALD) technique. The surface of the dielectric layer was chemically modified to help immobilize the Au NPs in aqueous solution. The modified substrate was immersed into the Au NP colloid. By controlling the dipping time, the density of NPs on the sample surface can be controlled. Fig. 4b and c show the transmission electron microscopy (TEM) images of the NPOM structure. The SiO$_2$ spacer layer of 2 nm thick is clearly observed. Due to the low density of the NPs, the coupling between NPs is negligible, and EM field enhancement results from the coupling between Au NPs and the Au film. Fig. 4d shows that the NPOM structure ("A") was SERS active, while the NP on the SiO$_2$/Si substrate ("B") produced no discernible Raman signal. The calculated electric field distribution in the NPOM system (Fig. 4e) shows that hot spot is generated in the nanogap between the NP and the Au film. With an increase of the spacer layer thickness, the Raman intensity drops rapidly. In addition, the SERS intensity is dependent on the angle of incidence of the laser light. A maximum SERS intensity is observed when the angle of incidence is 60° from the surface normal, which is caused by the interference of the incident and reflected field components. By increasing the Au NP density, NP aggregates were formed and hot spots between NPs were created. A strong SERS signal was observed from the region without the Au mirror. However, the SERS signal from the NPOM region was about 10 times stronger than that from the region without the Au mirror, which indicates the NPOM structure can efficiently increase SERS intensity for NPs of arbitrary density. As a SERS substrate the NPOM
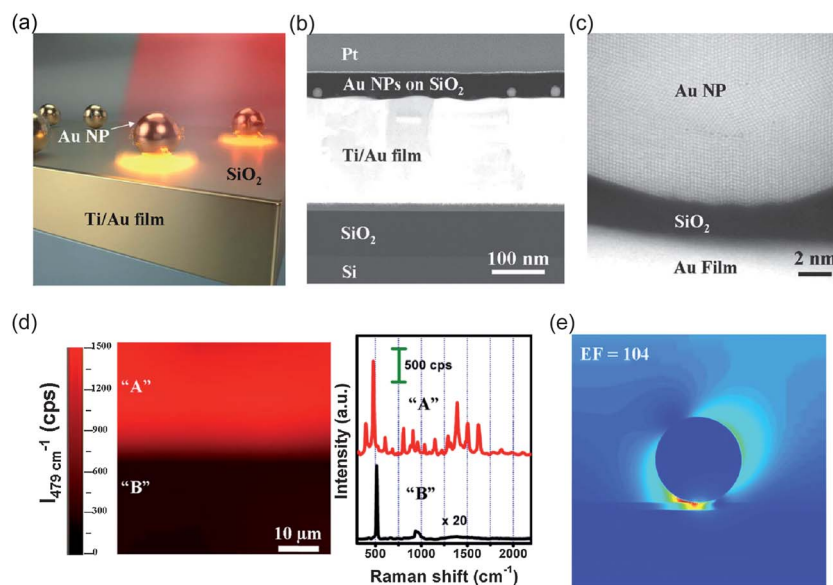
Fig. 4 (a) Schematic and (b) cross sectional HAADF STEM images of Au-NP near a gold film separated by a thin dielectric spacer deposited using the ALD technique. (c) High-resolution TEM image of an individual Au-NP on a 2 nm SiO_2 spacer showing its clear separation from the underlying Au film. (d) SERS spectral maps of two regions of the substrate. The first ("A") is the NPOM; the second ("B") is a region where the Au-NPs are deposited on the SiO_2/Si surface with no Au film. Representative SERS spectra of each region are shown to the right. The strong Raman line at ~520 cm^{-1} is due to Si. (e) Calculated spatial distribution of the electric field with 633 nm excitation for a Au NPOM assuming a 3 nm SiO_2 layer. (Reproduced from ref. 43.)

system can be easily fabricated with a large area, which is favorable for practical sensing applications. Other systems with metal nanostructures coupled to metal films, for instance gold nanostars over gold films, and silver and gold nanowires over silver or gold films, have also been explored as SERS platforms.[44,45]

2.2 NP dimer/chain and *in situ* SERS study of single dimer

Metal NP dimers are effective structures with large Raman enhancement factor. Methods for the high-throughput fabrication of NP dimers are desirable for SERS applications. By using a nanopatterning method and a meniscus force deposition technique, large arrays of NP dimers can be produced (Fig. 5a). To prepare the NP dimer arrays, nanohole arrays are firstly etched onto the silica-coated silicon substrate. A capillary force deposition method is applied to position the nanoparticles into the nanoholes. The nanohole-patterned substrate is treated by plasma to make the surface hydrophilic, and is then immersed in an aqueous gold NP colloid. As the aqueous solution is evaporated in a temperature-controlled environment, the meniscus slowly recedes across the substrate and NPs are positioned into the nanoholes at the contact line (Fig. 5a). The size of the nanohole determines that it can only hold two NPs, so dimer structures are obtained on the substrate (middle panel in Fig. 5a). The circular holes lead to a random orientation of the dimers. To make dimer arrays with a definite orientation, elongated nanoholes need to be fabricated. The bottom panel in Fig. 5a shows a NP dimer array with a well defined orientation by making elongated nanohole arrays on the substrate using focused ion beam milling.[46] For dimers of

Au NPs with diameter of 60 nm, the experimentally estimated enhancement factor of SERS is about 10^8 to 10^9.

By controlling the dimensions of the nanoholes or trenches on the substrates, a linear NP structure composed of different number of NPs can be fabricated.[47] The inset in Fig. 5b shows the SEM images of NP chains with one to nine NPs. The experimental results show that the NP dimer shows considerable Raman enhancement. For chains composed of more than two NPs, no additional enhancement is obtained. The calculation results by generalized Mie theory show that the NP dimer produces the largest Raman enhancement. With the increase of the length of the chain, the enhancement factor drops because the plasmon resonances shift to longer wavelengths. The dependence of the enhancement factor on the NP number is reproduced by some structures in experiments. The different behavior of the NP chains should be caused by the detailed morphology of the structures, which cannot be controlled accurately by the current nanofabrication method. Other methods to make NP chains have also been developed, for example by using a polymer shell to aggregate NPs, and by using DNA molecules and a molecular combing method.[9,48]

The EM field enhancement in the dimer structure is strongly dependent on the separation of the two particles. For small NPs, the EM enhancement is increased with the decrease of the separation of the dimer. However, when the separation is too small, quantum tunneling effects can reduce the EM field enhancement.[49] For larger particles, the separation dependence is different from that of small particles due to the excitation of multipolar resonances.[50] Since the detailed geometry differences of metal NP dimers can strongly influence the enhancement factor, it is not reliable to test the separation dependence
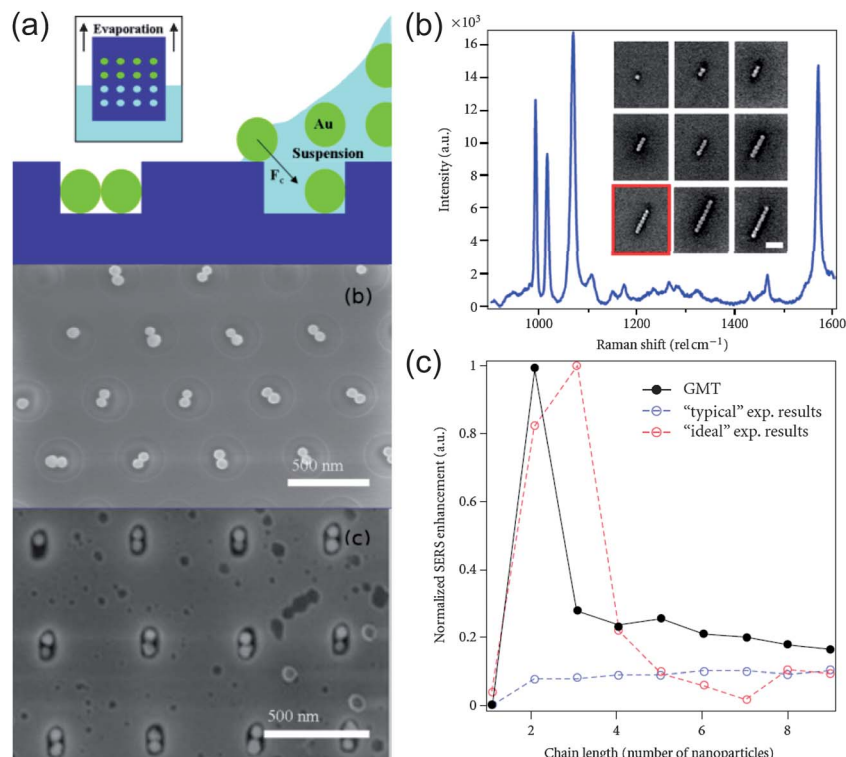
Fig. 5 (a) Top: schematic illustration of the capillary force (F_c) assembly mechanism at the vapor–suspension–substrate three-phase contact line. Middle and bottom: SEM images of the fabricated gold dimer arrays. (b) SERS spectrum of benzenethiol on a nanochain comprised of 60 nm gold nanospheres. Measurements were taken with 632.8 nm laser light polarized parallel to the nanochain axis. The inset shows the SEM images of gold nanochains ranging 1–9 particles in length. Scale bar is 300 nm. (c) Normalized SERS enhancement as a function of the chain length. Black: generalized Mie theory calculations. Blue and red: experimental results. (Reproduced from ref. 46 and 47.)

using different NP dimer structures. It is required that a single dimer structure can be actively and reversibly manipulated to change the gap distance to investigate the influence of the gap size on the Raman enhancement. A method that controlled the strain on an elastomeric substrate to control the separation of a dimer was reported.[50] Au–Ag–Au nanorods were prepared by electrochemical deposition in 200 nm diameter anodic alumina oxide (AAO) templates. Two Au rods of length 1 micron were separated by a Ag spacer layer of 80 nm thickness. The Au–Ag–Au heterostructured nanorods were dropcast on a prestrained silicone rubber substrate. By etching away the Ag, Au nanorod dimers were obtained on the elastomeric substrate. By controlling the strain of the substrate, control of the interparticle gap was realized. With the increase of the gap size, the SERS enhancement factor shows more than one peak, which originates from the multipolar resonances in the nanorods and is consistent with the results of electromagnetic simulations. The scattering properties of the Au NP dimers were also investigated for varied interparticle gaps modulated by stretching the elastomeric substrate.[51]

2.3 NP antennas manipulating the light polarization

Metal NP aggregates can not only enhance the intensity of the Raman scattering of probe molecules, but also influence the polarization of the Raman signal. As mentioned before, a NP

dimer is the simplest structure with a hot spot for SERS with single molecule sensitivity. For a dimer composed of two Ag NPs (Fig. 6a), its Raman enhancement is dependent on the polarization of the incident light.[52] For a single molecule in the nanogap of the dimer, the Raman intensity is strongest when the laser is polarized along the dimer axis, and weakest when the laser is polarized perpendicular to the dimer axis (middle panel in Fig. 6a). The polarization of the emitted Raman signal was analyzed for various incident polarizations. The result (right panel in Fig. 6a) shows that the maximum depolarization ratio ($\pm$1) was obtained when the incident laser polarized parallel to the dimer axis. Therefore, the emitted Raman scattered light is linearly polarized along the dimer axis. This polarization behavior is independent of the emission wavelength.[53]

For a NP trimer as shown in Fig. 6b, there are three possible locations for the single molecule, *i.e.* the three junctions formed by the three NPs. The plot of Raman intensity *vs.* incident polarization (middle panel in Fig. 6b) shows that the maximum Raman intensity is obtained when the incident polarization angle θ is about 75°, which is not along any NP pair. Calculations using generalized Mie theory (GMT) were performed by assuming the molecule is in each of the junctions. When the molecule is in the junction between particles 2 and 3 (Fig. 6b), the calculation results agree well with the experimental results. The presence of NP 1 makes the maximum Raman intensity
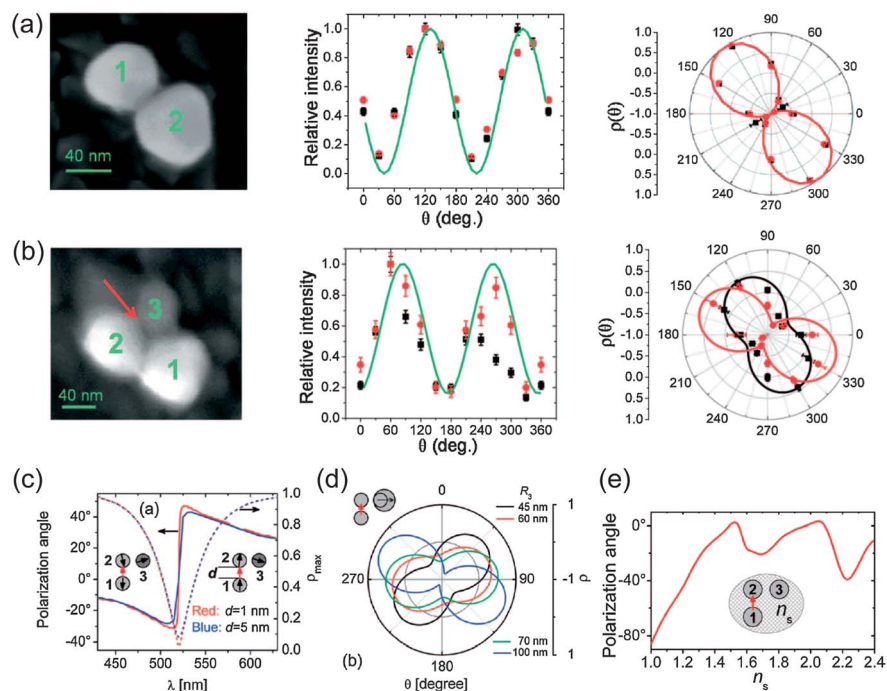
Fig. 6 (a) Polarization response of a NP dimer. Left: SEM image of a dimer. Middle: normalized Raman intensity at 555 nm (black squares) and 583 nm (red circles) as a function of the angle of rotation of the incident polarization. The green line is the result of a GMT calculation. Right: depolarization ratio measured at 555 nm (black squares) and 583 nm (red circles). Black and red lines show the results of GMT calculations performed at 555 and 583 nm, respectively. (b) Polarization response of a NP trimer. (c) Polarization angle (solid lines and left axis) and the maximum depolarization ratio (dashed lines and right axis) as a function of the wavelength of the dipole (denoted by a red arrow) emission for the right-angle configuration of a Ag trimer antenna with identical NPs (radius $R = 40$ nm). The separation between the 2nd and 3rd NPs is kept at 1 nm. (d) Depolarization ratio of light emitted from a right-angle Ag trimer with increasing radius of the third NP: $R_1 = R_2 = 40$ nm, $R_3 = 45, 60, 70,$ and 100 nm. Separations between NPs are kept at 1 nm. The wavelength of the dipole emission is 555 nm. The refractivity of the surrounding medium is 1. (e) Polarization angle of the emission from a right angle trimer ($R_1 = R_2 = 40$ nm, $R_3 = 80$ nm) as a function of the refractivity of the surrounding medium n_s. The wavelength of the dipole emission is 555 nm. Separations between NPs are kept at 1 nm. (Reproduced from ref. 53 and 54.)

deviate from the polarization along the axis of the particle 2 and 3. The polarization dependence of the Raman intensity shows no wavelength dependence. For the depolarization ratio, a clear wavelength dependence was observed (right panel in Fig. 6b). The maximum depolarization ratio was not obtained at the incident polarization corresponding to maximum Raman intensity. Another feature is that the depolarization ratio cannot reach ± 1 in the trimer case, which indicates that the emitted Raman scattering light is elliptically polarized.

The polarization rotation effect is strongly dependent on the position and size of the third particle (the particle 1 in Fig. 6b). Detailed theoretical studies reveal that, to rotate the emission polarization, the trimer structure must be asymmetric. For a trimer composed of three NPs of same radius of 40 nm (the inset in Fig. 6c), a dipole source is put in the junction of particle 1 and 2. If the third NP is put close to the dimer forming a new symmetric structure, for instance, the three particle is in a line or in an equilateral triangle configuration, the polarization of the emitted light is along the axis of the dimer (composed of particle 1 and 2). Only in an asymmetric configuration is the emission rotated. Fig. 6c shows the wavelength dependence of the polarization rotation of the emitted light. For short wavelength, the rotation is anticlockwise, while for a longer wavelength, the rotation becomes clockwise. Increasing the size of the third NP can increase the rotation angle of the emission

polarization (Fig. 6d). Apart from the geometrical parameters, the refractive index of the surrounding medium also has a significant influence on the polarization angle. Fig. 6e shows the variation of the polarization angle for media of different refractive index. As can be seen, the emission polarization is very sensitive to the refractive index change, which provides a means to modulate the emission polarization at the nanometer scale by controlling the refractive index of the medium.[54] Moreover, the NP antenna can also modulate the emission direction of the Raman signal.[55]

3 Nanostructure arrays

Nanostructure arrays prepared by nanofabrication techniques show prominent EM field enhancement. Due to the uniformity and the high reproducibility of the substrate, this kind of SERS substrate is quite promising for practical applications. By using porous aluminum oxide as template and an electrochemical deposition technique, metal nanorod arrays can be fabricated. Fig. 7a and b show the SEM images of two Ag nanorod arrays with different nanorod diameters and gap distances. The diameter and gap distance are determined by the size of the pore in the porous aluminum oxide, which can be controlled by the etching conditions. When excited by laser light of 785 nm wavelength, the inter-rod nanogaps provide the SERS hot spots.
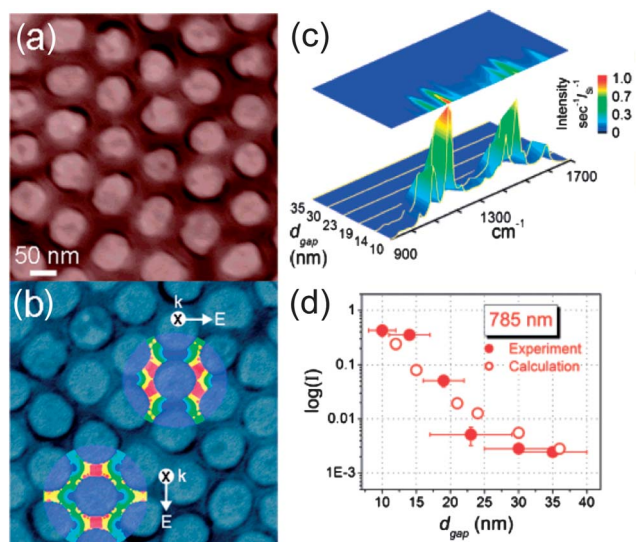
Fig. 7 (a and b) SEM images of Ag nanorods in templates. The calculated local electric field amplitudes in the vicinity of a central nanodisc surrounded by six hexagonally arranged discs are superimposed on the SEM image in (b). (c) SERS spectra and corresponding 2D intensity contour maps of 4-aminobenzenethiol (4-ABT) adsorbed on the Ag nanorod arrays are shown as a function of the inter-rod gap size d_{gap} for 785 nm excitation. (d) Experimentally measured (filled points) and calculated (open points) intensities of the 1078 cm^{-1} SERS line of 4-ABT plotted as a function of the inter-rod gap size. (Reproduced from ref. 56.)

The SERS intensity is increased over 200-fold when the inter-rod distance is decreased from 35 nm to 10 nm (Fig. 7c and d). The calculated electric field amplitude was overlaid on the SEM image in Fig. 7b. As can be seen, for different incident light polarizations the distribution of the hot spots is different. However, the averaged EM enhancement factor over the sample surface is independent of the laser polarization, which makes the experimental measurements unrestricted by the polarization of the laser light.[56]

By using the nanoimprint lithography technique, periodic nanostructure arrays can be made at large areas. Fig. 8a shows the SEM image of a dual-layer metallic grating (DMG) structure.[57] The grating structure was first transferred to the resist layer on an SiO$_2$-coated Si wafer, then a layer of Cr was deposited. After the lift-off process, a Cr mask was ready for the etching of SiO$_2$ by using reactive ion etching (RIE). By controlling the etching time, the height of the SiO$_2$ grating h_1 can be controlled. Gold was finally deposited onto the SiO$_2$ grating, and a dual-layer Au grating structure was obtained. The experimental measurements of SERS for gratings of different SiO$_2$ height h_1 show that the SERS enhancement factor is strongly dependent on the SiO$_2$ height. As shown in Fig. 8b, the gratings of SiO$_2$ height 330 nm and 165 nm generate much stronger SERS signal compared with the grating of SiO$_2$ height 275 nm and 550 nm. The 2D FDTD simulations show similar enhancement dependence on the SiO$_2$ height. Fig. 8c shows the calculated electric field distributions for gratings of $h_1 = 150$ nm and 220 nm, respectively. Hot spots are generated at the corners of the gold strips, which leads to the large Raman enhancement. The experimentally measured enhancement
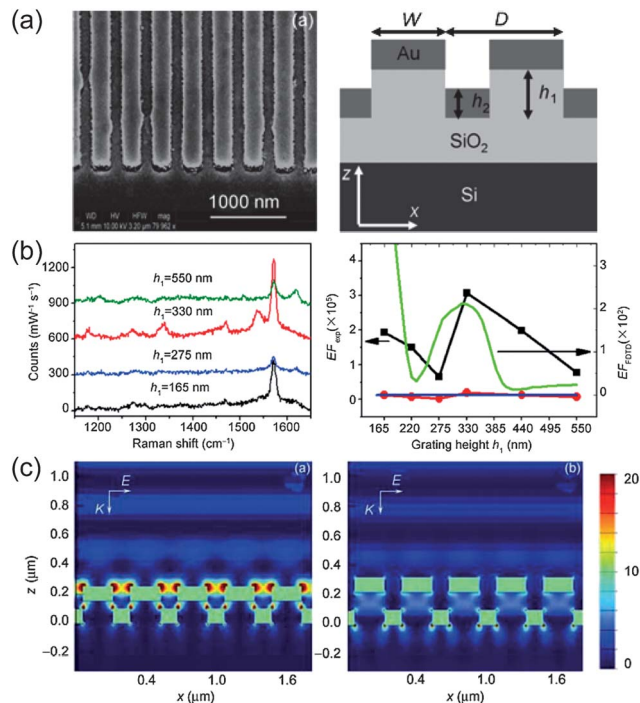

Fig. 8 (a) Left: tilted SEM image of gold DMG structure for $h_1 = 165$ nm, $D = 400$ nm, $w = 250$ nm, and $h_2 = 100$ nm. Right: schematic plot of the structure. (b) Left: Raman spectra of benzenethiol molecule on DMG structures for $h_1 = 165$ nm (black), 275 nm (blue), 330 nm (red) and 550 nm (olive), with the baseline subtracted for p-polarized incident light. Right: experimental and calculated enhancement factors as a function of SiO$_2$ grating heights h_1 for p- (black and green) and s-polarized (red and blue) incident light. (c) Calculated electric field amplitude |E| distribution, in the x–z plane for DMG structures with $h_1 = 150$ nm (left) and $h_1 = 220$ nm (right). (Reproduced from ref. 57.)

factor of SERS is as large as 10^5, which makes the dual-layer metallic grating structure a sensitive substrate for chemical sensing applications. Besides, the grating structures show good uniformity and repeatability of Raman enhancement over the whole grating area. As the nanoimprinting technique has the advantage of high throughput and low cost, the periodic metallic structures made by nanoimprinting are good candidates as high-performance SERS substrates.

To decrease the separation between adjacent nanowires, Deng *et al.* deposited additional SiO$_2$ onto the original SiO$_2$ grating before the deposition of gold.[58] More complex hierarchical periodic structures, such as butterfly wings have also been employed for fabricating SERS substrates.[59]

4 Structures with rough surfaces

Rough metal surfaces can generate an enhanced electromagnetic field. Most of the SERS experiments in the early years were performed on rough metal surfaces. With the progress in nanostructure fabrication, various nano/micro metal structures can be fabricated controllably. Fig. 9 shows some Ag structures with different surface topography prepared by chemical synthesis.[60,61] All these structures can be used to enhance Raman scattering. As there are many "hot spots" distributed on
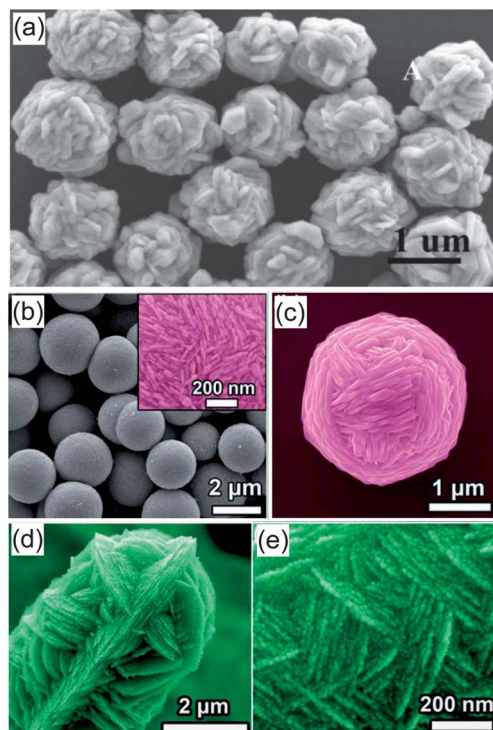
Fig. 9 (a–c) SEM images of Ag microparticles with different morphology. (d and e) SEM images of Ag wires for different magnification. (Reproduced from ref. 60 and 61.)

these highly textured structures, a single particle can efficiently enhance the Raman signals. Usually, the enhancement of these structures is less dependent on the polarization of the excitation light, which facilitates their application for SERS.[60–62] These particles are usually in the micron scale, so that they can be easily discerned under the optical microscope. By using a micromanipulator mounted on an optical microscope, these particles can be conveniently manipulated. A dimer structure can be formed by moving one particle to another. The SERS signal from the dimer was found to be much higher than that from an isolated particle before manipulating to the dimer.[63] This shows that although single particles can generate a detectable Raman signal, the coupling between particles still contributed dominantly to the total Raman enhancement in the aggregated particles. The self-assembled monolayer of such particles can form uniform substrates with sensitive SERS responses.[64]

5 Graphene-mediated SERS substrates

To promote the application of SERS in sensing, SERS substrates with high sensitivity, high reproducibility and high stability are required. If the analytes directly contact the metal surface, the interaction between the analytes and metal may disturb the pristine Raman signal. Li *et al.* developed a method which they call SHINERS (shell-isolated nanoparticle-enhanced Raman spectroscopy), which utilizes metal NPs coated with a dielectric layer (such as SiO_2, Al_2O_3) to enhance the Raman signals of

molecules. The dielectric layer can prevent the direct contact of molecules and metal surfaces to preclude signals induced by molecule–metal interactions.

Recently, Xu *et al.* reported a graphene-mediated SERS substrate (G-SERS substrate for short).[65] As shown in Fig. 10a, the probe molecules were deposited on silica/silicon substrate followed by transfer of one monolayer of graphene, and metal islands were finally deposited. By comparing the SERS spectra from Au and Ag nanoislands without and with monolayer graphene (Fig. 10b), it can be seen that the spectra from G-SERS substrates are much cleaner with pronounced Raman peaks corresponding to R6G molecules, while the spectra from normal SERS substrates show many additional and nonreproducible peaks (marked by red arrows) and a strong background around $1500 cm^{-1}$. The comparison of the spectra from G-SERS substrates and normal SERS substrates with no probe molecules shows that the former provides a cleaner baseline and the latter shows strong background (Fig. 10c) which may be caused by the photocarbonizaiton of the adsorbates from the atmosphere and the photoluminescence of the metal structure. Measurements over long time periods show that the intensity of spectra from the area with no graphene decrease with time, while the spectra from the area with graphene are quite stable (Fig. 10d).

The graphene layer can separate the molecules from the metal surface, and prevent possible photochemical processes which may degrade the probe molecules and generate a strong background. In addition, the graphene can effectively quench photoluminescence, which helps to generate a clean baseline.[66] Moreover, the orientation of molecules on flat graphene surfaces is much less complicated compared with that on the gold nanoislands film, which further simplifies the SERS spectra. In the sample structure shown in Fig. 10a, the electromagnetic field enhancement between adjacent nanoislands makes hot spots distribute on the flat graphene surface. Thus the molecules at the hot spots generate strongly enhanced Raman scattering. These studies show that the enhancement factor of the G-SERS substrate is comparable with the normal SERS substrate.

Xu *et al.* further developed a general type of G-SERS substrate (called G-SERS tape), which is transparent and freestanding. The monolayer graphene was grown on a copper foil by the chemical vapor deposition method. Metal nanoislands were then deposited followed by the spin coating of poly(methyl methacrylate) (PMMA). Finally the copper foil was etched away, resulting in the G-SERS tape of a layered structure of PMMA/metal/graphene. This kind of flexible SERS substrate can be applied to surfaces of arbitrary morphology for noninvasive and sensitive Raman analyses.

In the sample preparation process, if the metal island film is deposited first followed by the transfer of graphene, the graphene is then on the top surface of the nanoislands. In this configuration, the hot spots are far from the flat graphene surface, resulting in low Raman enhancement for the molecules on top of the graphene surface. Xu *et al.* recently reported a method using thermal annealing to reform the contact between the nanoislands and graphene.[67] After the annealing, the graphene was not a flat surface but wrinkled, following the
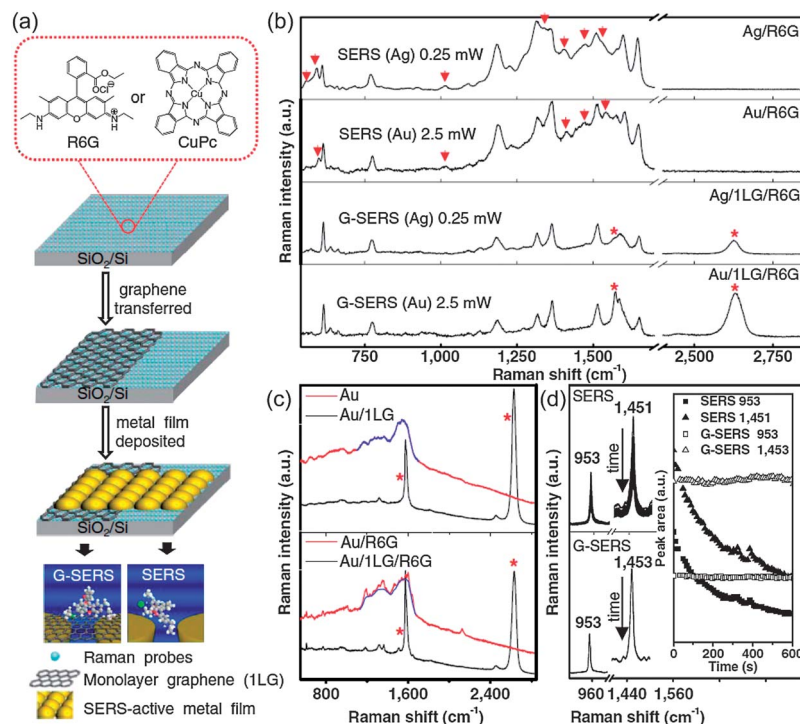
Fig. 10 Comparison of signals from a G-SERS substrate and a normal SERS substrate. (a) Schematic route for sample preparation with G-SERS and SERS regions on a SiO$_2$/Si substrate. (b) SERS and G-SERS spectra of R6G with gold and silver nanoislands used for enhancing the electromagnetic field, respectively. Red arrows here point to additional and nonreproducible peaks in spectra of normal SERS. (c) Photocarbonization effect (which causes a background at 1100–1700 cm^{-1}) in SERS and G-SERS substrates. (d) Stability of the SERS (top) and G-SERS (bottom) spectra of CuPc in a time series of 600 s. The inset shows the change of integrated intensity of the peaks (at 953 and 1451 cm^{-1} for SERS, and 953 and 1453 cm^{-1} for G-SERS, respectively) with the increased acquisition time. Time sequence: from top to bottom. "*" in (b) and (c) marks the G-band (∼1570 cm^{-1}) and G'-band (∼2625 cm^{-1}) of monolayer graphene. (Reproduced from ref. 65.)

morphology of the nanoisland film. In this case, the probe molecules can reach the hot spots. Therefore, stronger SERS signals were obtained.

The coverage of graphene on metal structures provides a passivated surface which prevents the interaction between metal and molecules. Compared with normal SERS experiments performed on a metal surface, the spectra from the G-SERS substrate is cleaner and more stable. The high performances of the G-SERS substrates and advanced techniques for graphene preparation make the graphene-mediated SERS substrates quite promising for practical SERS applications in analyses and detection. Aimed at the real-life application of SERS, researchers have developed various flexible SERS substrates, for instance, SERS test paper.[68–70] Polavarapu and Liz-Marzán have recently reviewed the progress on these low-cost flexible substrates.[71]

6 Tip-enhanced Raman spectroscopy (TERS)

Besides the various metal structures with hot spots for SERS, metal tips on scanning probe microscopes have also been employed to enhance Raman scattering, which has formed a new technique called tip-enhanced Raman spectroscopy (TERS).[72] The precise control of the metal tip makes the Raman enhancement process more controllable, and the tip–analyte separation can be controlled to examine the detailed influence

of the tip on the Raman enhancement. Additionally, the small size of the tip provides TERS with high spatial resolution, as the enhancement is mainly confined to the vicinity of the tip apex. Scanning probe microscopy can even resolve the image of a single molecule on the surface to realize *in situ* measurements of the single-molecule image and the Raman spectrum from the molecule. Liu *et al.* investigated single-molecule conductance and Raman spectra from molecular junctions by using a "fishing mode" TERS system.[73]

The metal tip alone cannot generate EM field enhancement as high as in NP aggregates. To improve the enhancement factor, metal films are usually used as substrates to support the analyte molecules. The coupling between the tip and the film generates a strong electric field in the cavity formed between them.[74] Chen *et al.* explored the TERS properties on Au films with Au NPs.[75] The experimental geometry is schematically shown in Fig. 11a. The coupling between the Au tip and Au NP (regarded as a fixed tip) makes a double-tip TERS setup. The Au tip is mounted on a scanning tunneling microscope (STM) and scanned over the sample surface. Laser light of 633 nm wavelength is focused on the Au tip through an objective. Raman signals are collected by the same objective. The STM image in Fig. 11a shows the Au films with Au NPs. Fig. 11b shows five TERS spectra of the probe molecules measured on different positions of the sample, which correspond to the five positions on the STM scanning profile in Fig. 11c. Prominent Raman
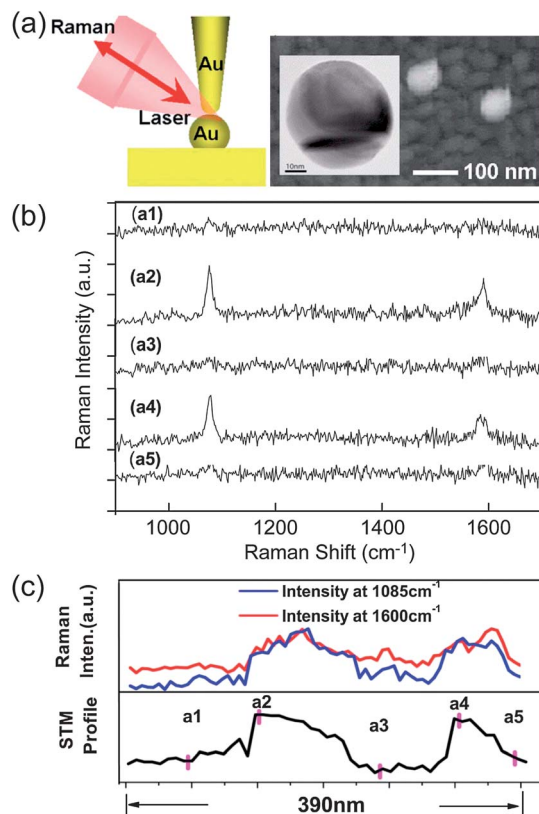
Fig. 11 (a) Illustration of a double-tip TERS setup. (b) Series of Raman spectra of *p*-thiocresol molecules collected from the positions marked in the STM profile in (c). (c) Top: scanned Raman intensity profiles at 1085 cm^{-1} (blue) and 1600 cm^{-1} (red), respectively, corresponding to the STM profile of the same scanning at the bottom. Bottom: STM profile where the Raman spectra were acquired. (Reproduced from ref. 75.)
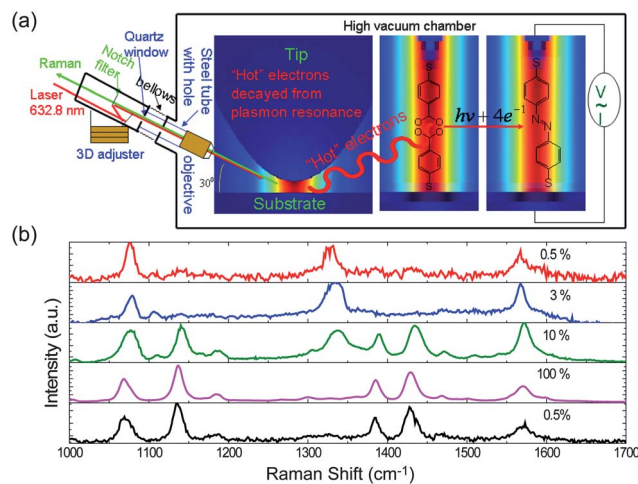

Fig. 12 (a) The design of a home-made HV-TERS setup. The Raman spectroscopy system is connected to a high vacuum chamber by a stainless steel bellow valve. A long working distance objective (NA = 0.5) in the high vacuum chamber is used for excitation and collection of Raman signals at the nanogap between the STM tip and the substrate. (b) The spectral dependence on laser power. Laser power was tuned to be 0.5%, 3%, 10%, 100% and 0.5% of the full power in time sequence for the spectra from top to bottom. The bias voltage is 1 V, and the tunneling current is 1 nA. (Reproduced from ref. 76.)

peaks for *p*-thiocresol were obtained at positions a2 and a4, where Au NPs were located. These results show that, for the excitation wavelength used in the experiment, the coupling between the tip and the NP generates a stronger Raman enhancement compared with the tip–film coupling.

Recently, Sun *et al.* demonstrated in a high vacuum tip-enhanced Raman spectroscopy (HV-TERS) setup that the surface plasmons in the coupled Au tip–Ag film structure can catalyze the chemical reaction of dimerizing 4-nitro-benzenethiol (4NBT) to dimercaptoazobenzene (DMAB) (Fig. 12a).[76] The TERS spectra of the molecules were measured at different laser powers. At low laser power, the spectra show the Raman peaks corresponding to vibrations in 4NBT molecules (red and blue spectra in Fig. 12b). With the laser power increased to 10%, additional peaks appeared, which can be assigned to DMAB. When the laser power was increased to 100%, the Raman peak at 1336 cm^{-1} disappeared, indicating all the 4NBT molecules in the detection area have been dimerized to DMAB. When the laser power was greatly decreased, the spectrum still shows the Raman peaks of DMAB molecules (black spectrum in Fig. 12b). In addition, IR-active vibrational modes and Fermi resonances of DMAB were also observed in the HV-TERS system.[77]

7 Conclusions and outlook

In this feature article, we have reported some recent progresses on surface-/tip-enhanced Raman spectroscopy, covering the enhancement properties, remote-excitation technique, manipulation of the emission polarization of the probe molecules, different kinds of metal nanostructures made with different methods, graphene-mediated SERS substrates, TERS for tip–nanoparticle coupled systems, and the chemical reactions revealed by the high vacuum TERS setup. Plasmon-enhanced Raman spectroscopy has become a versatile method for label-free detection of small amounts of analytes. The essence of fabricating various SERS substrates is to tailor the "hot spots" in metal nanostructures. The size, density and distribution of the hot spots determine the enhancement performance of the SERS substrates. Therefore, the reproducible generation of hot spots is an indispensable requirement for the development of superior SERS substrates.

To get experimentally more details about hot spots, super-resolution imaging methods have been developed to study single hot spots in aggregated NPs beyond the resolution limit set by the diffraction of light. Willets and coworkers have conducted a series of work to resolve the individual hot spots using single molecule SERS.[78,79] The resolution they have achieved is better than 5 nm, which can provide detailed information about the size, shape and electric field distribution of the hot spots. These studies also provide information about the chemical dynamics properties of single molecules, as the emission intensity and positions of the single molecule are continuously recorded at the hot spot. Single molecule studies avoid the ensemble average effect, and give insights into the interaction between a single molecule and a single hot spot.

Besides the ability to detect tiny molecules, the strongly enhanced electromagnetic field in the hot spots can interact with the molecules to result in specific phenomena, for instance, the plasmon-assisted chemical reactions of molecules,[80] in which case the hot spots on one hand catalyze the chemical reaction and on the other hand make the reaction detectable *in situ*. This subject is becoming active and may accelerate the penetration of SERS into the field of chemistry.

The combination of SERS and other techniques can facilitate application. SERS can be integrated with micro-/nano-fluidic techniques to detect the analytes in the liquid flowing through the fluidic devices. This incorporation improves the sensitivity of the micro-/nano-fluidic devices and expands the applications of SERS, which can lead to highly efficient lab-on-a-chip sensing devices.[81-83] SERS can also combine with surface plasmon resonance (SPR) sensing techniques to realize simultaneous measurements of SERS and SPR.[84] It was demonstrated that SERS properties can be actively controlled using multiferroic substrates. The dielectric properties of the substrate can be tuned by the applied voltage, so that the SERS enhancement can be modulated.[85] By incorporating metal nanostructures with other high-performance materials and by integrating SERS/TERS with other techniques, the applications of plasmon-enhanced Raman spectroscopy will be further promoted.

Acknowledgements

References

1 M. Fleischmann, P. J. Hendra and A. J. McQuillan, *Chem. Phys. Lett.*, 1974, **26**, 163–166.

2 D. L. Jeanmaire and R. P. Van Duyne, *J. Electroanal. Chem.*, 1977, **84**, 1–20.

3 K. Kneipp, M. Moskovits and H. Kneipp, *Surface-Enhanced Raman Scattering*, Physics and Applications, New York, 2006.

4 H. X. Xu, E. J. Bjerneld, M. Kall and L. Borjesson, *Phys. Rev. Lett.*, 1999, **83**, 4357–4360.

5 H. X. Xu, J. Aizpurua, M. Kall and P. Apell, *Phys. Rev. E: Stat. Phys., Plasmas, Fluids, Relat. Interdiscip. Top.*, 2000, **62**, 4318–4324.

6 H. X. Xu, *Appl. Phys. Lett.*, 2004, **85**, 5980–5982.

7 H. X. Xu, X. H. Wang, M. P. Persson, H. Q. Xu, M. Kall and P. Johansson, *Phys. Rev. Lett.*, 2004, **93**, 243002.

8 D. K. Lim, K. S. Jeon, H. M. Kim, J. M. Nam and Y. D. Suh, *Nat. Mater.*, 2009, **9**, 60–67.

9 G. Chen, Y. Wang, M. X. Yang, J. Xu, S. J. Goh, M. Pan and H. Y. Chen, *J. Am. Chem. Soc.*, 2010, **132**, 3644–3645.

10 H. X. Xu and M. Kall, *Phys. Rev. Lett.*, 2002, **89**, 246802.

11 F. Svedberg, Z. P. Li, H. X. Xu and M. Kall, *Nano Lett.*, 2006, **6**, 2639–2641.

12 S. Y. Lee, L. Hung, G. S. Lang, J. E. Cornett, I. D. Mayergoyz and O. Rabin, *ACS Nano*, 2010, **4**, 5763–5772.

13 P. H. C. Camargo, L. Au, M. Rycenga, W. Y. Li and Y. N. Xia, *Chem. Phys. Lett.*, 2010, **484**, 304–308.

14 F. Hao, C. L. Nehl, J. H. Hafner and P. Nordlander, *Nano Lett.*, 2007, **7**, 729–732.

15 C. Hrelescu, T. K. Sau, A. L. Rogach, F. Jackel and J. Feldmann, *Appl. Phys. Lett.*, 2009, **94**, 153113.

16 H. Wei, A. Reyes-Coronado, P. Nordlander, J. Aizpurua and H. X. Xu, *ACS Nano*, 2010, **4**, 2649–2654.

17 E. C. Le Ru, J. Grand, I. Sow, W. R. C. Somerville, P. G. Etchegoin, M. Treguer-Delapierre, G. Charron, N. Felidj, G. Levi and J. Aubard, *Nano Lett.*, 2011, **11**, 5013–5019.

18 N. A. Hatab, C. H. Hsueh, A. L. Gaddis, S. T. Retterer, J. H. Li, G. Eres, Z. Y. Zhang and B. H. Gu, *Nano Lett.*, 2010, **10**, 4952–4955.

19 V. G. Kravets, G. Zoriniants, C. P. Burrows, F. Schedin, C. Casiraghi, P. Klar, A. K. Geim, W. L. Barnes and A. N. Grigorenko, *Phys. Rev. Lett.*, 2010, **105**, 246806.

20 K. D. Osberg, M. Rycenga, N. Harris, A. L. Schmucker, M. R. Langille, G. C. Schatz and C. A. Mirkin, *Nano Lett.*, 2012, **12**, 3828–3832.

21 D.-K. Lim, K.-S. Jeon, J.-H. Hwang, H. Kim, S. Kwon, Y. D. Suh and J.-M. Nam, *Nat. Nanotechnol.*, 2011, **6**, 452–460.

22 R. W. Taylor, T. C. Lee, O. A. Scherman, R. Esteban, J. Aizpurua, F. M. Huang, J. J. Baumberg and S. Mahajan, *ACS Nano*, 2011, **5**, 3878–3887.

23 Y. H. Zheng, T. Thai, P. Reineck, L. Qiu, Y. M. Guo and U. Bach, *Adv. Funct. Mater.*, 2013, **23**, 1519–1526.

24 L. Gunnarsson, E. J. Bjerneld, H. Xu, S. Petronis, B. Kasemo and M. Kall, *Appl. Phys. Lett.*, 2001, **78**, 802–804.

25 O. Balmes, J. O. Bovin, J. O. Malm and H. X. Xu, *Vib. Spectrosc.*, 2005, **37**, 189–193.

26 X. J. Liu, L. A. Zhao, H. Shen, H. X. Xu and L. H. Lu, *Talanta*, 2011, **83**, 1023–1029.

27 M. P. Cecchini, V. A. Turek, J. Paget, A. A. Kornyshev and J. B. Edel, *Nat. Mater.*, 2012, **12**, 165–171.

28 J. N. Chen, T. Martensson, K. A. Dick, K. Deppert, H. Q. Xu, L. Samuelson and H. X. Xu, *Nanotechnology*, 2008, **19**, 275712.

29 K. Singhal and A. K. Kalkan, *J. Am. Chem. Soc.*, 2010, **132**, 429–431.

30 A. Yashchenok, A. Masic, D. Gorin, B. S. Shim, N. A. Kotov, P. Fratzl, H. Mohwald and A. Skirtach, *Small*, 2013, **9**, 351–356.

31 E. A. Vitol, Z. Orynbayeva, M. J. Bouchard, J. Azizkhan-Clifford, G. Friedman and Y. Gogotsi, *ACS Nano*, 2009, **3**, 3529–3536.

32 Y. R. Fang, Y. Z. Li, H. X. Xu and M. T. Sun, *Langmuir*, 2010, **26**, 7737–7746.

33 A. G. Brolo, E. Arctander, R. Gordon, B. Leathem and K. L. Kavanagh, *Nano Lett.*, 2004, **4**, 2015–2018.

34 Q. Z. Hao, Y. Zeng, B. K. Juluri, X. D. Wang, B. Kiraly, I. K. Chiang, L. Jensen, D. H. Werner, V. H. Crespi and T. J. Huang, *ACS Nano*, 2011, **5**, 5472–5477.

35 Z. L. Yang, Q. H. Li, B. Ren and Z. Q. Tian, *Chem. Commun.*, 2011, **47**, 3909–3911.

36 H. Wei, U. Hakanson, Z. L. Yang, F. Hook and H. X. Xu, *Small*, 2008, **4**, 1296–1300.

37 F. M. Huang, D. Wilding, J. D. Speed, A. E. Russell, P. N. Bartlett and J. J. Baumberg, *Nano Lett.*, 2011, **11**, 1221–1226.

38 H. Wei, F. Hao, Y. Z. Huang, W. Z. Wang, P. Nordlander and H. X. Xu, *Nano Lett.*, 2008, **8**, 2497–2502.

39 T. Kang, S. M. Yoo, I. Yoon, S. Y. Lee and B. Kim, *Nano Lett.*, 2010, **10**, 1189–1193.

40 H. Wei and H. X. Xu, *Nanophotonics*, 2012, **1**, 155–169.

41 Y. R. Fang, H. Wei, F. Hao, P. Nordlander and H. X. Xu, *Nano Lett.*, 2009, **9**, 2049–2053.

42 J. A. Hutchison, S. P. Centeno, H. Odaka, H. Fukumura, J. Hofkens and H. Uji-i, *Nano Lett.*, 2009, **9**, 995–1001.

43 S. Mubeen, S. P. Zhang, N. Kim, S. Lee, S. Kramer, H. X. Xu and M. Moskovits, *Nano Lett.*, 2012, **12**, 2088–2094.

44 L. Rodriguez-Lorenzo, R. A. Alvarez-Puebla, I. Pastoriza-Santos, S. Mazzucco, O. Stephan, M. Kociak, L. M. Liz-Marzán and F. J. G. de Abajo, *J. Am. Chem. Soc.*, 2009, **131**, 4616–4618.

45 I. Yoon, T. Kang, W. Choi, J. Kim, Y. Yoo, S. W. Joo, Q. H. Park, H. Ihee and B. Kim, *J. Am. Chem. Soc.*, 2009, **131**, 758–762.

46 K. D. Alexander, M. J. Hampton, S. P. Zhang, A. Dhawan, H. X. Xu and R. Lopez, *J. Raman Spectrosc.*, 2009, **40**, 2171–2175.

47 K. D. Alexander, S. P. Zhang, A. R. Hight Walker, H. X. Xu and R. Lopez, *J. Nanotechnol.*, 2012, **2012**, 840245.

48 H. Wei and H. Xu, *Appl. Phys. A: Mater. Sci. Process.*, 2007, **89**, 273–275.

49 L. Mao, Z. P. Li, B. Wu and H. X. Xu, *Appl. Phys. Lett.*, 2009, **94**, 243102.

50 K. D. Alexander, K. Skinner, S. P. Zhang, H. Wei and R. Lopez, *Nano Lett.*, 2010, **10**, 4488–4493.

51 F. M. Huang and J. J. Baumberg, *Nano Lett.*, 2010, **10**, 1787–1792.

52 H. X. Xu and M. Kall, *ChemPhysChem*, 2003, **4**, 1001–1005.

53 T. Shegai, Z. P. Li, T. Dadosh, Z. Y. Zhang, H. X. Xu and G. Haran, *Proc. Natl. Acad. Sci. U. S. A.*, 2008, **105**, 16448–16453.

54 Z. P. Li, T. Shegai, G. Haran and H. X. Xu, *ACS Nano*, 2009, **3**, 637–642.

55 T. Shegai, B. Brian, V. D. Miljkovic and M. Kall, *ACS Nano*, 2011, **5**, 2036–2041.

56 S. J. Lee, Z. Q. Guan, H. X. Xu and M. Moskovits, *J. Phys. Chem. C*, 2007, **111**, 17985–17988.

57 Z. Q. Guan, U. Hakanson, N. Anttu, H. Wei, H. Q. Xu, L. Montelius and H. X. Xu, *Chin. Sci. Bull.*, 2010, **55**, 2643–2648.

58 X. G. Deng, G. B. Braun, S. Liu, P. F. Sciortino, B. Koefer, T. Tombler and M. Moskovits, *Nano Lett.*, 2010, **10**, 1780–1786.

59 Y. W. Tan, J. J. Gu, X. N. Zang, W. Xu, K. C. Shi, L. H. Xu and D. Zhang, *Angew. Chem., Int. Ed.*, 2011, **50**, 8307–8311.

60 H. Y. Liang, Z. P. Li, W. Z. Wang, Y. S. Wu and H. X. Xu, *Adv. Mater.*, 2009, **21**, 4614–4618.

61 B. Zhang, P. Xu, X. M. Xie, H. Wei, Z. P. Li, N. H. Mack, X. J. Han, H. X. Xu and H. L. Wang, *J. Mater. Chem.*, 2011, **21**, 2495–2501.

62 F. Z. Cong, H. Wei, X. R. Tian and H. X. Xu, *Front. Phys.*, 2012, **7**, 521–526.

63 H. Y. Liang, Z. P. Li, Z. X. Wang, W. Z. Wang, F. Rosei, D. L. Ma and H. X. Xu, *Small*, 2012, **8**, 3400–3405.

64 J. X. Fang, S. Y. Du, S. Lebedkin, Z. Y. Li, R. Kruk, M. Kappes and H. Hahn, *Nano Lett.*, 2010, **10**, 5006–5013.

65 W. G. Xu, X. Ling, J. Q. Xiao, M. S. Dresselhaus, J. Kong, H. X. Xu, Z. F. Liu and J. Zhang, *Proc. Natl. Acad. Sci. U. S. A.*, 2012, **109**, 9281–9286.

66 L. M. Xie, X. Ling, Y. Fang, J. Zhang and Z. F. Liu, *J. Am. Chem. Soc.*, 2009, **131**, 9890–9891.

67 W. G. Xu, J. Q. Xiao, Y. F. Chen, Y. B. Chen, X. Ling and J. Zhang, *Adv. Mater.*, 2013, **25**, 928–933.

68 C. H. Lee, L. M. Tian and S. Singamaneni, *ACS Appl. Mater. Interfaces*, 2010, **2**, 3429–3435.

69 R. Zhang, B. B. Xu, X. Q. Liu, Y. L. Zhang, Y. Xu, Q. D. Chen and H. B. Sun, *Chem. Commun.*, 2012, **48**, 5913–5915.

70 C. L. Zhang, K. P. Lv, H. T. Huang, H. P. Cong and S. H. Yu, *Nanoscale*, 2012, **4**, 5348–5355.

71 L. Polavarapu and L. M. Liz-Marzán, *Phys. Chem. Chem. Phys.*, 2013, **15**, 5288–5300.

72 B. Pettinger, P. Schambach, C. J. Villagomez and N. Scott, in *Annual Review of Physical Chemistry*, 2012, vol. 63, pp. 379–399.

73 Z. Liu, S. Y. Ding, Z. B. Chen, X. Wang, J. H. Tian, J. R. Anema, X. S. Zhou, D. Y. Wu, B. W. Mao, X. Xu, B. Ren and Z. Q. Tian, *Nat. Commun.*, 2011, **2**, 305.

74 Z. L. Yang, J. Aizpurua and H. X. Xu, *J. Raman Spectrosc.*, 2009, **40**, 1343–1348.

75 J. N. Chen, W. S. Yang, K. Dick, K. Deppert, H. Q. Xu, L. Samuelson and H. X. Xu, *Appl. Phys. Lett.*, 2008, **92**, 093110.

76 M. T. Sun, Z. L. Zhang, H. R. Zheng and H. X. Xu, *Sci. Rep.*, 2012, **2**, 647.

77 M. T. Sun, Y. R. Fang, Z. Y. Zhang and H. X. Xu, *Phys. Rev. E: Stat., Nonlinear, Soft Matter Phys.*, 2013, **87**, 020401.

78 S. M. Stranahan and K. A. Willets, *Nano Lett.*, 2010, **10**, 3777–3784.

79 K. A. Willets, *Phys. Chem. Chem. Phys.*, 2013, **15**, 5345–5354.

80 M. T. Sun and H. X. Xu, *Small*, 2012, **8**, 2777–2786.

81 L. M. Tong, M. Righini, M. U. Gonzalez, R. Quidant and M. Kall, *Lab Chip*, 2009, **9**, 193–195.

82 Y. J. Oh, S. G. Park, M. H. Kang, J. H. Choi, Y. Nam and K. H. Jeong, *Small*, 2011, **7**, 184–188.

83 Y. Yin, T. Qiu, W. J. Zhang and P. K. Chu, *J. Mater. Res.*, 2011, **26**, 170–185.

84 Y. Liu, S. P. Xu, B. Tang, Y. Wang, J. Zhou, X. L. Zheng, B. Zhao and W. Q. Xu, *Rev. Sci. Instrum.*, 2010, **81**, 036105.

85 X. Y. Xu, K. Seal, X. S. Xu, I. Ivanov, C. H. Hsueh, N. Abu Hatab, L. F. Yin, X. Q. Zhang, Z. H. Cheng, B. H. Gu, Z. Y. Zhang and J. A. Shen, *Nano Lett.*, 2011, **11**, 1265–1269.